

Modeling Multi-Granularity Context Information Flow for Pavement Crack Detection

Junbiao Pang, Baocheng Xiong, Jiaqi Wu

Abstract—Crack detection has become an indispensable, interesting yet challenging task in the computer vision community. Specially, pavement cracks have a highly complex spatial structure, a low contrasting background and a weak spatial continuity, posing a significant challenge to an effective crack detection method. In this paper, we address these problems from a view that utilizes contexts of the cracks and propose an end-to-end deep learning method to model the context information flow. To precisely localize crack from an image, it is critical to effectively extract and aggregate multi-granularity context, including the fine-grained local context around the cracks (in spatial-level) and the coarse-grained semantics (in segment-level). Concretely, in Convolutional Neural Network (CNN), low-level features extracted by the shallow layers represent the local information, while the deep layers extract the semantic features. Additionally, a second main insight in this work is that the semantic context should be an guidance to local context feature. By the above insights, the proposed method we first apply the dilated convolution as the backbone feature extractor to model local context, then we build a context guidance module to leverage semantic context to guide local feature extraction at multiple stages. To handle label alignment between stages, we apply the Multiple Instance Learning (MIL) strategy to align the high-level feature to the low-level ones in the stage-wise context flow. In addition, compared with these public crack datasets, to our best knowledge, we release the largest, most complex and most challenging Bitumen Pavement Crack (BPC) dataset. The experimental results on the three crack datasets demonstrate that the proposed method performs well and outperforms the current state-of-the-art methods.

Index Terms—crack detection, multi-scale, context information, spatial structure

I. INTRODUCTION

PAVEMENT crack is one of the most potential yet important factors that endanger road safety, which constantly erode the internal structure of the road. Pavement cracks have produced a series of hazards, seriously affecting the life of the infrastructure, especially for the large number of highways. As a consequence, with the increasing length of roads, the accurate detection of cracks is increasingly becoming a vital method to not only maintain the safety of roads but also extend the life of roads. Efficient crack detection method is a practical requirement especially for bitumen pavement.

The core issue of crack detection is to achieve the precise crack localization and area. As shown in Fig. 1, both the

unique structure and the special appearance the cracks pose significant challenges. Specially, bitumen pavement as a mix of bitumen and gravels naturally forms a crack-like road surface. Fig. 1 illustrates that the low contrast between cracks and background, weak continuity of cracks, and complex noise interference with cracks make a significant challenges to the practical crack detection tasks, especially for the bituminous pavement roads as follows:

- 1) **Low contrast:** Small and unclear cracks have a low contrast with the background. Besides, the high similarity between the cracks and the background makes many cracks too difficult to be accurately labeled.
- 2) **Weak continuity:** The crack has a group of structures with a irregular and weak continuity distribution. It indicates that cracks would occur at any position on roads.
- 3) **Noise interference:** The background contains complex noises, such as the spots with different shapes and the scratches with varying lengths. These crack-like noises seriously affect the performance of crack detection methods.

Both semantic segmentation [1] [2] and object detection [3] [4] are the two mainstream methods for the crack detection task. However, due to the unique spatial structure of cracks, we find that both methods have their drawbacks. For the segmentation approach, pixel-level result guarantees the precise crack detection, but it requires the pixel-level annotations which cause a significant amount of time consumption. As shown in Fig. 1 (a), cracks in the red rectangle are almost impossible to be accurately labeled pixel-level labeling. For the object detection method, it requires a bounding box to label the crack positions. However, the bounding box barely reflects the weak continuity of cracks, being unable to accurately label and measure the detailed cracks.

Compared to the semantic segmentation approach and the object detection one, as illustrated in Fig. 1 (b), patch-level annotation is an approach to balance between efficiency and accuracy. That is, the patch-level annotation significantly reduces the difficulty of annotation. It seems that if an image patch is considered as a pixel, approaches from the semantic segmentation approach can readily be used for the crack detection. However, the patch-level annotation contains significant more noises than that of the pixel-level annotation, as illustrated in Fig. 1 (b). These annotation makes the approaches for the semantic segmentation task inefficiently for crack detection. For instance, U-Net [2] predicts multiple results by easily converting pixel-level annotation into the

Manuscript created October, 2020; This work was developed by the IEEE Publication Technology Department. This work is distributed under the L^AT_EX Project Public License (LPPL) (<http://www.latex-project.org/>) version 1.3. A copy of the LPPL, version 1.3, is included in the base L^AT_EX documentation of all distributions of L^AT_EX released 2003/12/01 or later. The opinions expressed here are entirely that of the author. No warranty is expressed or implied. User assumes all risk.

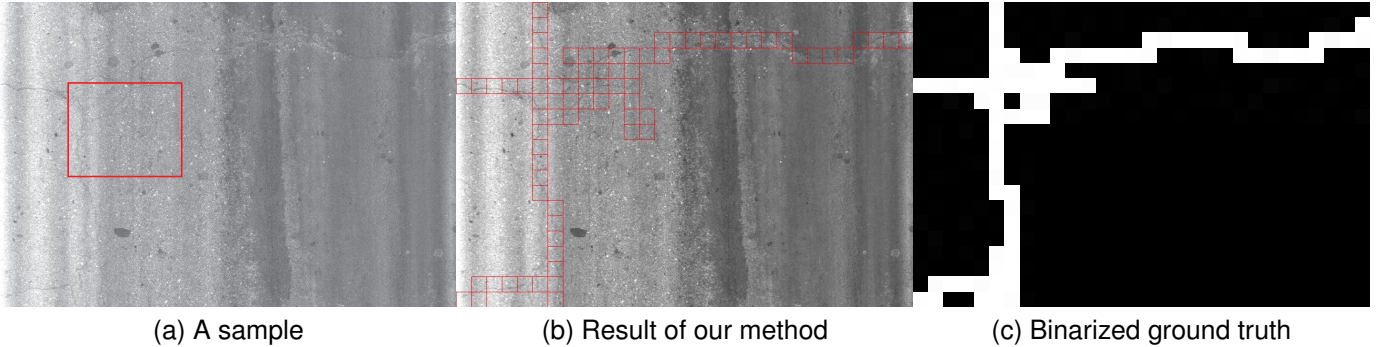


Fig. 1. A result of MGCrackNet on BPC. Cracks in the red rectangle are difficult labeled in Fig. 1(a), and please zoom out the image for the more detailed cracks.

different scales. However, the patch-level annotation barely generates the accurate ground truths for the different scales for U-Net.

In this paper, we propose to fuse **Multi Granularity** context information to model a **Crack** detection neural **Network** (MGCrackNet), as illustrated in Fig. 2. To our best knowledge, MGCrackNet firstly leverages the dilated convolution to extract more local context information, where local features (e.g. textural details of roads) and the spital information is captured to precisely locate cracks. Naturally, deep layers have more semantic information than that of the shallow ones [5]. Therefore, two granularity-level context are should be fused to model the context of cracks.

A natural idea is that the deep layers need the detailed spatial information to precisely detect cracks, while the shallow layers need to be guided by the semantic information of deep layers. To achieve this bootstrap-like procedure, we firstly freeze shallow layers and only optimize features from the deep layers. The advantage of this step is that semantic information can be a guidance information for the shallow layers. Secondly, we unfroze and optimize the shallow layers, forcing the multi-granularity context information to gradually optimize the features from the deep layers to shallow ones. Besides, to align the context cues from the the deep layers to shallow ones, we introduce Multiple Instance Learning (MIL) strategy [6][7][8] to further improve crack detection performance. Comparative experiments and ablation studies on three datasets demonstrate the proposed method achieves state-of-the-art performance, showing the superior ability of our network.

The contributions of this work are summarized in the two-fold:

- To our best knowledge, to handle the patch-level annotation, we firstly propose multi-granularity context information flow to gradually guide context cues from deep layers to shallow ones. Besides, the bootstrap-like training procedure is proposed to efficiently fuse context cues and local ones.
- To our best knowledge, we release the largest, the most complex and challenge bitumen pavement crack dataset, which adopts the patch-level annotation. It brings new and considerable challenges for the crack detection com-

munity.

II. RELATED WORK

Pixel-Level Crack Detection: Pixel-level crack detection is a semantic segmentation based method that aims accurately to recognize the crack pixels. The key to crack pixels recognition lies in distinguishing between cracks and background. For example, the physical property is a straightforward way for crack detection including spatial continuity [9] [10] [11]. Besides, fusing context information is an efficiency method [12] [13] [14] [15]. However, most of these cracks in the experiments are serious ones which are easily labeled cement pavement.

Due to the complex spatial structure of cracks, it is difficult to label cracks in a pixel wise approach. In practice, the industrial requirement pays attention to these mild yet unclear cracks, because the repair cost for these cracks is lower than that of these serious ones.

Region-Level Crack Detection: Region-level crack detection is an object detection based method that essentially judges whether there is a crack or not. For example, You Only Look Once v3 (YOLOv3) is combined with deformable convolution to locate cracks [4][16]. The method based on YOLOv5 construct 12 different attention models for crack detection [17]. In addition, [18] uses fast R-CNN to detect cracks in order to handling different weather conditions and lighting levels. [19] first uses Mask R-CNN coarse locate cracks and second determines the severity of crack damage.

The performance of the region-level crack detection is continuously improved with the progress of the object detection community. However, the predicted results are too imprecise to quantify the area of cracks. In fact, the method [20] just detects these serious cracks because they are easily be labeled.

Patch-Level Crack Detection: Patch level crack detection is a classification method that divides a crack image into multiple patches and further determines which patch is a crack. In [21], a deep CNN is proposed to classify the image patches. In [22] [23], context information from the different layers are used to improve the predicted results. In [24], the optimization of crack characteristics at each stage improves the crack detection performance, which adopts the idea of modeling context information.

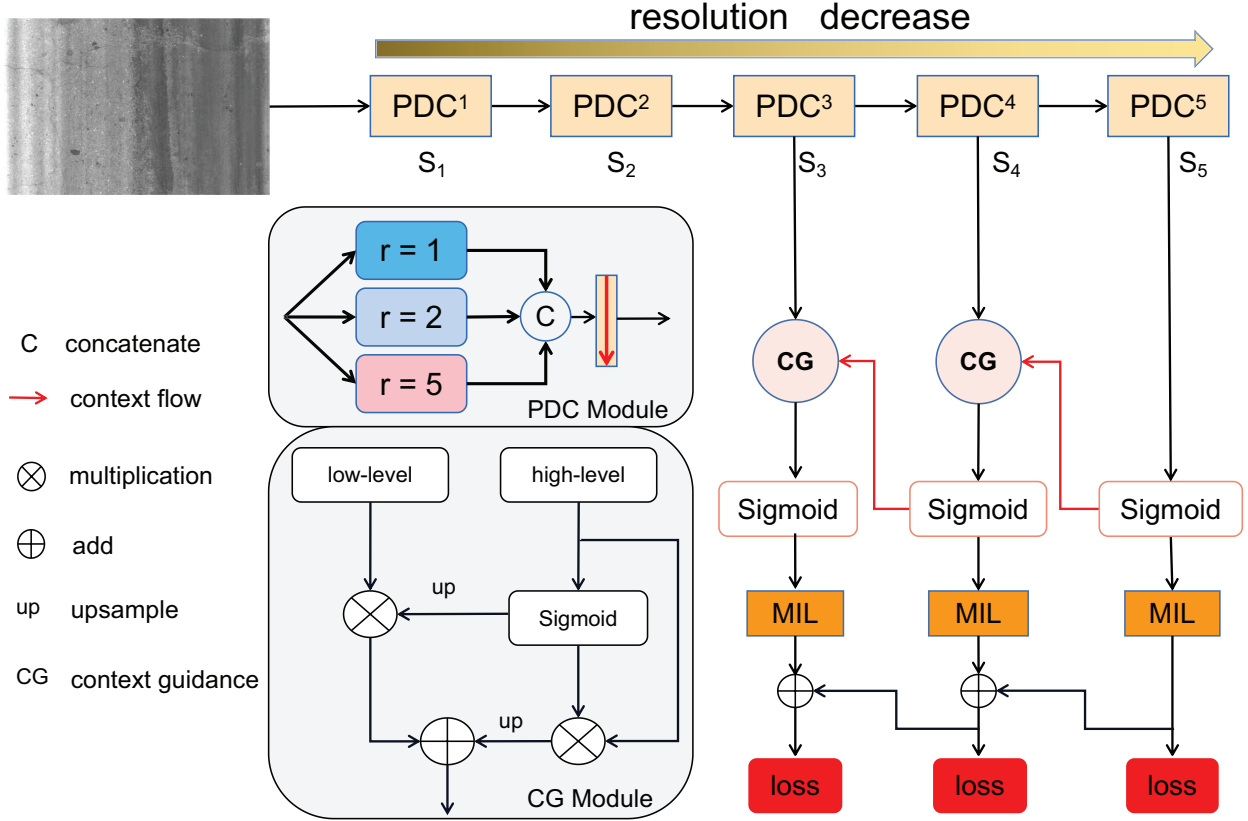


Fig. 2. The network structure of MGCrackNet, which is composed of context feature extraction stages, context guidance module, MIL strategy and loss function.

However, The above methods only rely on feature-level context and barely utilizes semantic contextual information. Besides, these methods ignore that the patch-level label is a weak annotation, which results in the inefficient feature extraction. Consequently, the context cues are inaccurate to efficiently improve detection performance. On the contrary, our Context Guidance (CG) module not only utilizes the context cues but also refines the feature extraction with the help of the MIL-based label alignment.

III. MODELING CONTEXT INFORMATION

A. MGCrackNet

In this paper, we adopt the parallel dilated convolution(PDC) [25] module to extract local context of cracks. As shown in the PDC module in Fig. 2, the PDC module is composed of 3 dilated convolutional layers with the dilated rates of $r \in \{1, 2, 5\}$ as follows:

$$O_r = C_r(F_i) \quad (1)$$

where F_i is the feature, $C_r(\cdot)$ is convolution operator with the dilated rate r . The dilated convolution (1) inserts holes (zero) to expand the size of convolution kernel, extracting more context features than that of the standard convolution. However, these holes also result in the loss of information. Concatenate features $S_o = \text{concat}(O_1, O_2, O_5)$ compensate for the loss of these holes in convolution.

The PDC naturally obtains a larger context than that of the standard convolution. As shown in Fig. 3, in a patch with cracks, only a small pixels belong to cracks, while other regions is background or noises. Finally, we apply the max-pooling operation to sub-sampling the result of PDC (1). We stack PDC and max-pooling as the backbone of network, as shown in Fig. 2.

As shown in Fig. 2, MGCrackNet further sperate the backbone of network into different stages.

Definition 1. (Stage). The Stage is a repeatable feature extraction module in a neural network. Usually, a stage consists of the combination of the convolution-pooling operations.

In this paper, we split the network into 5 stages S_i , ($i \in \{1, 2, 3, 4, 5\}$). Features extracted from 5 stages are respectively donated as $F_{S_i} \in \mathbb{R}^{\frac{1}{2^i}H \times \frac{1}{2^i}W \times C_i}$, ($C_i \in \{32, 64, 128, 256, 256\}$), ($i \in \{1, 2, 3, 4, 5\}$), where C_i is the number of channels for the i -th stage.

The previous approach [24] stacks several backbones of the network into a new network to boost the performance. However, stacking multiple backbones naturally lead to an over-load yet inefficient neural network during the training and the deployment stages. On the contrary, our stage-wise approach is more efficiently.

In this paper, we only use the feature maps of the last three stages, $F_{S_3} \in \mathbb{R}^{\frac{1}{8}H \times \frac{1}{8}W \times C_3}$, $F_{S_4} \in \mathbb{R}^{\frac{1}{16}H \times \frac{1}{16}W \times C_4}$ and $F_{S_5} \in \mathbb{R}^{\frac{1}{32}H \times \frac{1}{32}W \times C_5}$. Because the last three stages contain less noise interference [26]. Concretely, $F_{S_{i-1}}$ represents the

local context of cracks, F_{S_i} contains the high-level semantic information, but also include more noise interference [27]. Therefore, a reasonable approach is to combine the advantages of both high-level features and the low-level ones.

Consequently, we propose to model context information flow between two stages, where the semantic context guides the extraction of the local context of cracks. During the guidance procedure, we use MIL to align the annotation between two consecutive stages. By this process, we gradually optimize the feature maps at each stage with the same loss functions.

B. Context Guidance Module

The CG module leverages the context cues to help the shallower stage extract informative features and local context, as illustrated in Fig. 2. Concretely, the deeper stage generates a heatmap of cracks, where each value in the map means the probability of whether a patch contains a crack or not. Denote the features extracted by the stage S_i as F_{S_i} , the corresponding feature map M_{S_i} is computed as follows:

$$M_{S_i} = \sigma(F_{S_i}) \quad (2)$$

where $\sigma(\cdot)$ is the sigmoid function, index $i \in \{3, 4, 5\}$ and $m_{xy} \in M_{S_i}$ is the probability weights, $M_{S_i} \in \mathbb{R}^{H_{S_i} \times W_{S_i} \times C_i}$, ($H_{S_i} = \frac{1}{2^i}H, W_{S_i} = \frac{1}{2^i}W$), $m_{xy} \in [0, 1]$, $x = 1, \dots, H_{S_i}, y = 1, \dots, W_{S_i}$, where H_{S_i} and W_{S_i} are the number of the patches in a image.

The heatmap M_{S_i} acts as an attention mechanism to guide the feature extraction of the shallow layer, assigning a higher value to the crack position. Besides, the features F_{S_i} contain the context cues of the consecutive stage, because the receptive field of the stage S_i is larger than the stage S_{i-1} . Therefore, we further enhance the discriminative ability of feature F_{S_i} as follows:

$$\hat{F}_{S_i} = M_{S_i} \otimes F_{S_i} \quad (3)$$

where \otimes is the element-wise multiplication. Thus, the weighted feature \hat{F}_{S_i} is a self-refined feature.

To align the feature size between two consecutive stages, the heatmap M_{S_i} is upsampled through bilinear interpolation operation. The low-level feature $F_{S_{i-1}}$ is weighted by the upsampled heatmap $up(M_{S_i})$ as follows:

$$\hat{F}_{S_{i-1}} = up(M_{S_i}) \otimes F_{S_{i-1}} \quad (4)$$

where $up(\cdot)$ is the upsampling function.

If we consider M_{S_i} as the context of the stage S_{i-1} , $\hat{F}_{S_{i-1}}$ is the context guided features. Concretely, in (4), the element-wise multiplication guides feature $F_{S_{i-1}}$ to pay attention to the important positions in the receptive field of the shallow stage. To verify this assumption, the gradient of feature $\hat{F}_{S_{i-1}}$ with respect to parameters θ as follows:

$$\frac{\partial \hat{F}_{S_{i-1}}}{\partial \theta} = \frac{\partial up(M_{S_i})}{\partial \theta} \otimes F_{S_{i-1}} + up(M_{S_i}) \otimes \frac{\partial F_{S_{i-1}}}{\partial \theta} \quad (5)$$

where $\frac{\partial \cdot}{\partial \theta}$ is the gradient of the different features with respect to parameters θ .

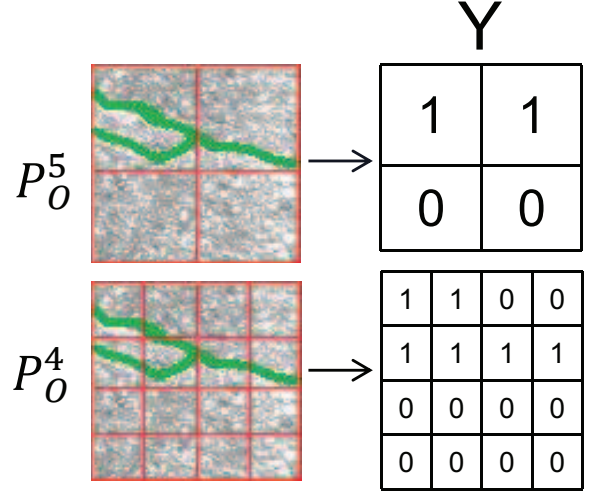


Fig. 3. A patch-level annotation across two consecutive stages.

Obviously, in (5), the gradient $\frac{\partial \hat{F}_{S_{i-1}}}{\partial \theta}$ is controlled by four terms, e.g. M_{S_i} , $\frac{\partial up(M_{S_i})}{\partial \theta}$, $F_{S_{i-1}}$, and $\frac{\partial F_{S_{i-1}}}{\partial \theta}$, in which the heatmap M_{S_i} is generated by the feature $F_{S_{i-1}}$ from the previous stage S_{i-1} . If we simultaneously optimize $F_{S_{i-1}}$ and M_{S_i} , a possible gradient contradicts would happen between $F_{S_{i-1}}$ and M_{S_i} . Consequently, the inaccurate heatmap M_{S_i} tends to fail guide the features for the shallow stages. Therefore, a natural yet effective strategy is firstly to freeze $F_{S_{i-1}}$ and optimize M_{S_i} as follows:

$$\frac{\partial \hat{F}_{S_{i-1}}}{\partial \theta} = \frac{\partial up(M_{S_i})}{\partial \theta} \otimes F_{S_{i-1}} \quad (6)$$

To retain the sufficient priors from the deeper stage and leverage the features from the shallow one, the upsampled feature $up(\hat{F}_{S_i})$ is element-wisely added to the features $\hat{F}_{S_{i-1}}$ from the shallow stage as follows:

$$F_{S_i}^o = add(up(\hat{F}_{S_i}), \hat{F}_{S_{i-1}}) \quad (7)$$

where $F_{S_i}^o$ is the weighted low-level feature at the stage S_i , and $add(\cdot, \cdot)$ is the element-wise addition operation.

C. Label Alignment for Stage-Wise Loss

An naive idea is that if we supervise network at the different stages, we will extract more discriminative features. However, the label alignment problem naturally happens, once we supervise the MGCrackNet at the different stages. Because the ground truth is annotated at the patch-wise granularity rather than the pixel-wise one. Consequently, we can not directly compute a loss at different stages. For example, as shown in Fig. 3, an 128×128 image is divided into 4×4 patches, where each 32×32 patch is labeled whether it contains a crack or not for the stage S_5 . Unfortunately, the annotation of the 16×16 sub-patches cannot be generated from the 4×4 patch-wise annotation. We call this problem as the label alignment problem.

We apply the MIL strategy to solve the label alignment problem. Concretely, a ‘‘bag’’ corresponds to a patch, while an ‘‘instance’’ corresponds to a sub-patch in a patch. A classifier

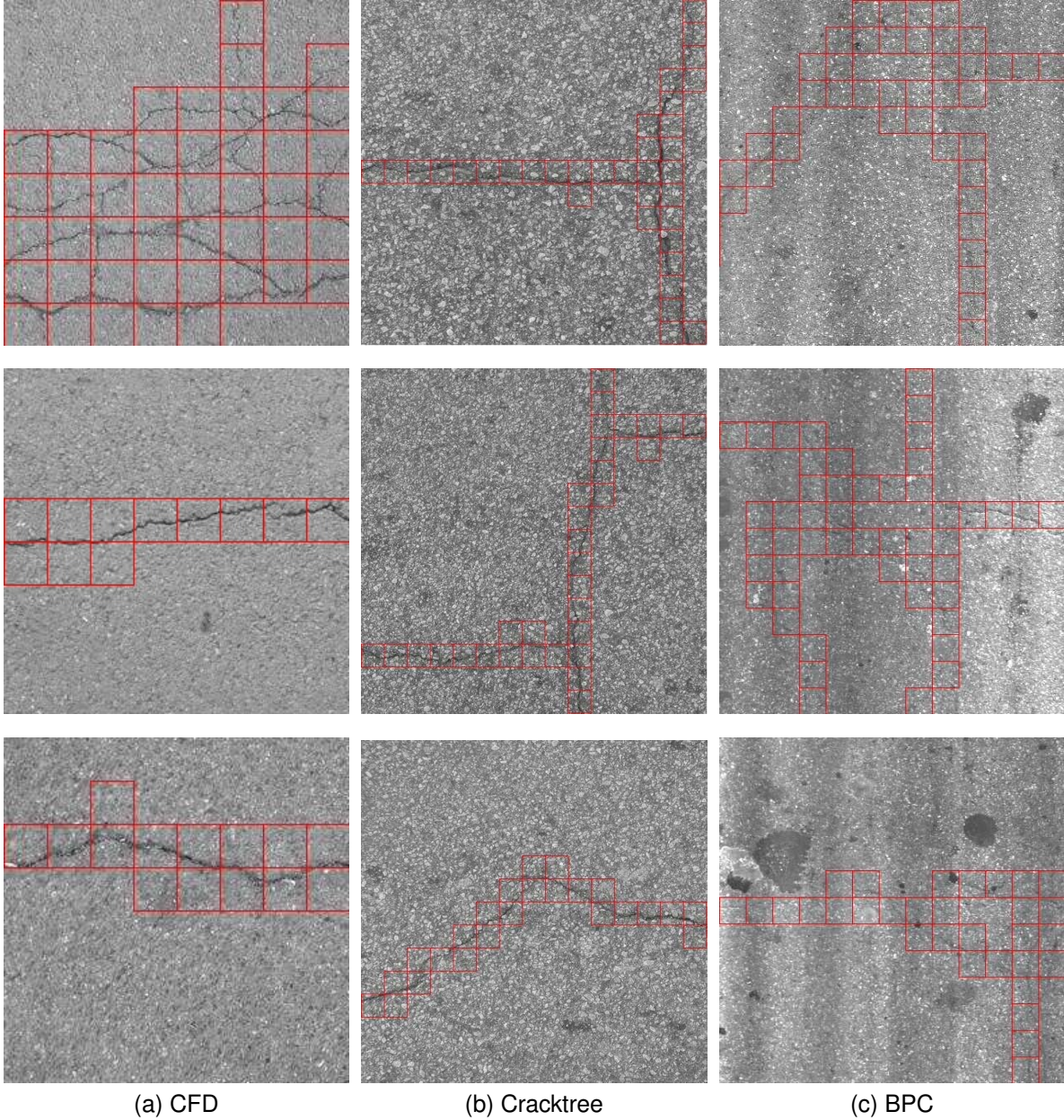


Fig. 4. Some samples from three datasets. The columns from the left to the right represent the ground truth of CFD, Cracktree and BPC dataset, respectively.

is firstly built by a 3×3 standard convolution and two 1×1 standard convolutions for each sub-regions as follows:

$$P_o^i = \sigma(F_{S_i}^o) \quad (8)$$

where $\sigma(\cdot)$ is the sigmoid function and P_o^i is the classification probability, $P_o^i \in \mathbb{R}^{\frac{1}{2^i}H \times \frac{1}{2^i}W \times C_i}$ for the stage S_i .

Secondly, MIL strategy is used to convert the probability P_o^i of the sub-regions to the patch-wise annotation as follows:

$$Y_o^i = pool(P_o^i) \quad (9)$$

where $pool(\cdot)$ is the pooling function, Y_o^i is the classification probability at the different stages, $Y_o^i \in \mathbb{R}^{\frac{1}{32}H \times \frac{1}{32}W \times C}$. In MGCrackNet, the function $pool(\cdot)$ uses stride $\{4, 2, 1\}$ for

the S_i , respectively. During inference, if the probability Y_o^i is greater than 0.5, it indicates that a patch contains cracks.

D. Loss function

We employ a multi-stage supervised approach to optimize the predicted results, as shown in Fig. 2. Concretely, given a labeled sample $\{X, Y\}$, where $X \in \mathbb{R}^{\frac{1}{2^i}H \times \frac{1}{2^i}W \times C}$ is an image, $Y \in \mathbb{R}^{\frac{1}{32}H \times \frac{1}{32}W \times C}$ is the corresponding multi-stage label, and $i \in \{3, 4, 5\}$ are index of the different stages, Cross Entropy (CE) loss of a sample $\{X, Y\}$ is used at different stages as follows:

$$L = \sum_{i=3}^5 CE(Y_o^i, Y) \quad (10)$$

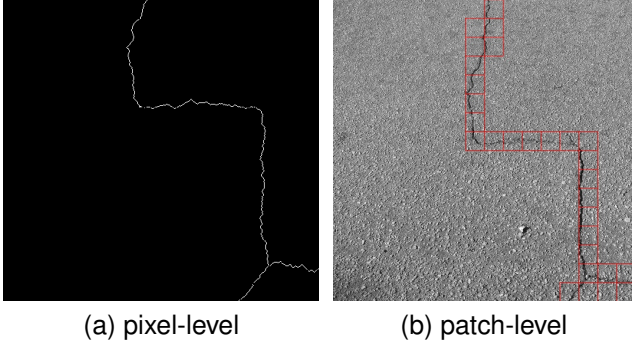


Fig. 5. The pixel-level annotation is converted into the the patch-level one.

where $CE(\cdot, \cdot)$ is the cross entropy loss.

IV. EXPERIMENTS

A. Dataset Comparisons

1) **CFD**: The CFD [28] dataset is for the cement road crack. CFD contains 118 crack images with a size of 480×320 . We use the 256×256 sliding window to crop the images, generating 2,832 samples, where 2,256 samples are used for the training and 576 ones are for the testing. Each sample is divided into 32×32 patches. Some samples from CFD are shown in Fig. 4 (a).

2) **Cracktree**: The Cracktree dataset is also for the cement road crack [29]. This dataset consists of 206 crack images with a size of 800×600 . We use the 512×512 sliding window to generate the 1,300 training samples and the 324 testing ones. Each samples is further divided into 32×32 patches. Some samples from Cracktree are shown in Fig. 4 (b).

3) **BPC**: We release the challengeable Bitumen Pavement Crack (BPC) dataset, which comprises 3,522 images with a size of 640×960 . Each image is divided into 16×16 patches with a size of 32×32 . We use the 416×416 sliding window to generate 7,044 samples, where the 5,764 training samples and the 1,280 testing ones. Some samples from BPC are shown in Fig. 4 (c). Rather than Cracktree and CFD, BPC contains about 3,080 noisy patches which are difficult to be correctly labeled by annotators. Because this problem is caused by the materials (e.g. the mix of bitumen and gravel) of the bitumen pavement itself.

Due to the complexity of bitumen pavement cracks, the cracks and background are highly similar, some of these patches barely be subjectively judged by humans (see Fig. 6). During the labeling process, we have investigated the experts to label these patches. These cracks make BPC challenge to the SOTA methods.

It should note that both CFD and Cracktree are the pixel-level annotation, which does not meet our setting. During experiments, we regenerate patch-level labels from the pixel-level annotation as shown in Fig. 5.

As compared with both public datasets, the purpose that we release BPC for the research community are two folds:

- The cracks of bitumen pavement are more changeable than that of the cement road. Our experimental results also confirm this observation.

TABLE I
COMPARISON BETWEEN THREE DATASETS

Attributes	BPC	CFD	Cracktree
Road Types	Bitumen	Cement	Cement
Image Size	$640 \times 960?$	480×320	800×600
Patch Size	32×32	32×32	32×32
Sliding Window	416×416	256×256	512×512
# Image	5764	2832	1624
# Noise Patches	3080	0	0
$\frac{\#BgPatch}{\#CrackPatch}$	16 : 1	3 : 1	6 : 1

- The patch-level crack detection, a weakly supervised approach, is a challenge yet practical problem. Reducing the annotation difficulty yet obtaining a satisfied accurate performance is a practical industrial requirement.

B. Evaluation Metrics

In this paper, $Precision(P)$ and $Recall(R)$ are adopted to evaluate the performances among different methods. The $F1$ score measures the performance from $Precision$ and $Recall$ as follows:

$$F1 = 2 \frac{P \cdot R}{P + R} \quad (11)$$

where P is $Precision$, R is $Recall$.

To further evaluate the performance of crack detection, $AveragePrecision(AP)$ of the cracks is computed as a comprehensive metric to reflect the overall stability of the model as follows:

$$AP = \int_0^1 P(t) dt \quad (12)$$

where value $P(t)$ is the precision P at the threshold t , $t \in [0, 1]$. Therefore, AP is equivalent to the area under the precision-recall curve, measures the performance of cracks rather than the background patches.

Algorithm 1 Freeze Training Strategy.

INPUT: multi-stage features $\{F_{S_i}, i \in 3, 4, 5\}$
iteration number $t = 1, \dots, N$
OUTPUT: feature map $\{Y_o^i, i \in 3, 4, 5\}$
 $Y_o^i | i = 3, 4, 5 \leftarrow F_{S_i}, i \in 3, 4, 5;$
for $t = 1; t < N; t \leftarrow t + 1$ **do**
 if $1 \leq t \leq 20$ **do**
 $Y_o^3, Y_o^4, Y_o^5 \leftarrow freeze(F_{S_3}), freeze(F_{S_4}), CG(F_{S_5});$
 if $20 < t \leq 40$ **do**
 $Y_o^3, Y_o^4, Y_o^5 \leftarrow freeze(F_{S_3}), CG(F_{S_4}), CG(F_{S_5});$
 if $40 < t \leq N$ **do**
 $Y_o^3, Y_o^4, Y_o^5 \leftarrow CG(F_{S_3}), CG(F_{S_4}), CG(F_{S_5});$
 end
return $\{Y_o^i\};$

TABLE II
CONTRASTING EXPERIMENTAL RESULTS ON THREE DATASETS

Methods	BPC				CFD				Cracktree			
	$P(\%)$	$R(\%)$	$F1(\%)$	$AP(\%)$	$P(\%)$	$R(\%)$	$F1(\%)$	$AP(\%)$	$P(\%)$	$R(\%)$	$F1(\%)$	$AP(\%)$
ST [30]	0.00	0.00	0.00	9.16	86.90	72.56	79.08	86.98	85.66	85.58	85.61	90.09
FT [31]	0.00	0.00	0.00	9.25	80.30	67.01	73.05	81.92	78.03	75.42	76.70	84.23
DenseNet121 [32]	53.86	64.64	58.75	61.46	91.20	79.60	85.00	90.05	89.26	87.22	88.22	93.67
ResNet50 [33]	76.70	78.69	77.68	79.41	94.68	84.53	89.31	93.64	93.34	83.97	89.55	93.23
VGG16 [34]	77.95	81.40	79.63	82.51	95.57	83.77	89.28	94.76	94.91	84.77	89.55	93.23
DCNN [21]	74.46	68.44	71.32	75.84	94.32	85.13	89.48	94.83	91.51	79.01	84.80	91.94
MSCNN [22]	77.58	72.85	75.14	80.20	96.93	85.52	90.91	96.57	92.93	83.97	88.22	93.85
UFE [35]	76.23	80.17	78.15	82.37	96.96	90.09	93.39	95.76	92.44	82.76	87.33	92.63
SFE [24]	84.71	73.35	78.62	85.10	96.17	85.82	90.70	95.62	92.55	89.93	91.22	92.99
MGCrackNet	86.90	72.45	79.02	88.32	97.21	90.35	93.65	97.29	90.21	90.17	90.19	95.24

C. Experiment Settings

In our experiments, we use the open-source deep learning framework PyTorch and conduct the tests on NVIDIA 3080 GPUs. During training, we do not use any pre-trained models instead train the models from the scratch. We set the batch size as 16 and use Stochastic Gradient Descent (SGD). Weight decay and momentum are set to 0.0005 and 0.9, respectively. We set the initial learning rate to $1e - 3$. After 40 epoches, it will be divided by 10 for every 20 epoches. we use data augmentation techniques such as random rotation, random cropping, and symmetric transformations to improve the model robustness.

In addition, we employ the freezing training strategy in Alg. 1. Concretely, we freeze low-level features in the first 20 epoches and only optimize high-level features, and then open lower-level features in turn for training every 20 epoches.

D. Baselines and The State-of-Art Approaches

To demonstrate the superiority of the proposed method, we compare MGCrackNet with different methods on these public datasets from three aspects as follows:

- **Global Semantic Context:** Two general vision transformer networks, Swin Transformer [30] (ST) and Focal Transformer [31] (FT), are used as baseline to extract the global context features. Based on the Transformer [36] architecture, ST and FT extract global context features from samples and achieve the best performance in visual classification tasks. Therefore, we use both methods as baselines to extract global semantic context features for crack detection.
- **Local Context:** Three efficient architectures, VGG16 [34], ResNet50 [33] and DenseNet121 [32], are used as baseline to extract local context features. These algorithms are also successful in visual classification tasks.
- **The State of Art Crack Detection Methods:** The State-Of-The-Art (SOTA) methods includes Deep Convolution Neural Network (DCNN) [21], Multi-Scale classification network (MSCNN) [22], Structural Feature Extraction model(SFE) [24], and Unconventional Feature Extraction model (UFE) [35]. These methods belong to patch-level crack detection algorithms. The reasons that we list them as SOTA methods as follows:

- **DCNN:** This paper detected cracks by a deep convolution network. However, this method ignores the importance of context information.
- **UFE and SFE:** Both UFE and SFE extract local context information by feature fusing strategy. However, these methods did not handle label alignment problem.
- **MSCNN:** This paper uses multiple max-pooling operations at different layers of the network to sub-sample the local feature. However, these max-pooling operations cause serious information loss.

For a fair comparison, the learning rate and the other hyper-parameters of these comparison methods are tuned to obtain the best performances for these STOA methods.

E. Experimental Results

1) *Results on CFD:* Tab. II shows that our method outperforms the other STOA methods in terms of both AP and $F1$. For instance, compared with DCNN, MSCNN, UFE and SFE, our method achieves 97.29% AP , which has 2.46%, 0.72%, 1.53% and 1.67% improvement, respectively. We notice that the CFD barely has label noise and the cracks are almost clear ones for the cement pavement. As expected, the AP of MSCNN, UFE and SFE also achieve excellent performances in Tab. II. As a comparison, our method achieves competitive performances over two evaluation criteria from $F1$ and AP metrics.

Another important observation is that UFE achieves the closest performance to our method in terms of P , R and $F1$, as illustrated in Fig. 7(b). Our method adopts the multi-stage context information flow to boost the discriminative ability of features. It indicates that multi-stage context cues is necessary for crack detection.

Either the global semantic context method (*i.e.*, ST and FT) or the local one does not obtain the comparative performances in Table II. One possible reason is that transformer based methods perform well for a large data sets with the diversified local appearances, which help robust use attention mechanism. However, the high similarity between the background and cracks damage this assumption, especially for the BPC dataset.

2) *Results on CrackTree:* Compared to the CFD dataset, the Cracktree dataset is more complex, due to the shadows, and the blurred background.

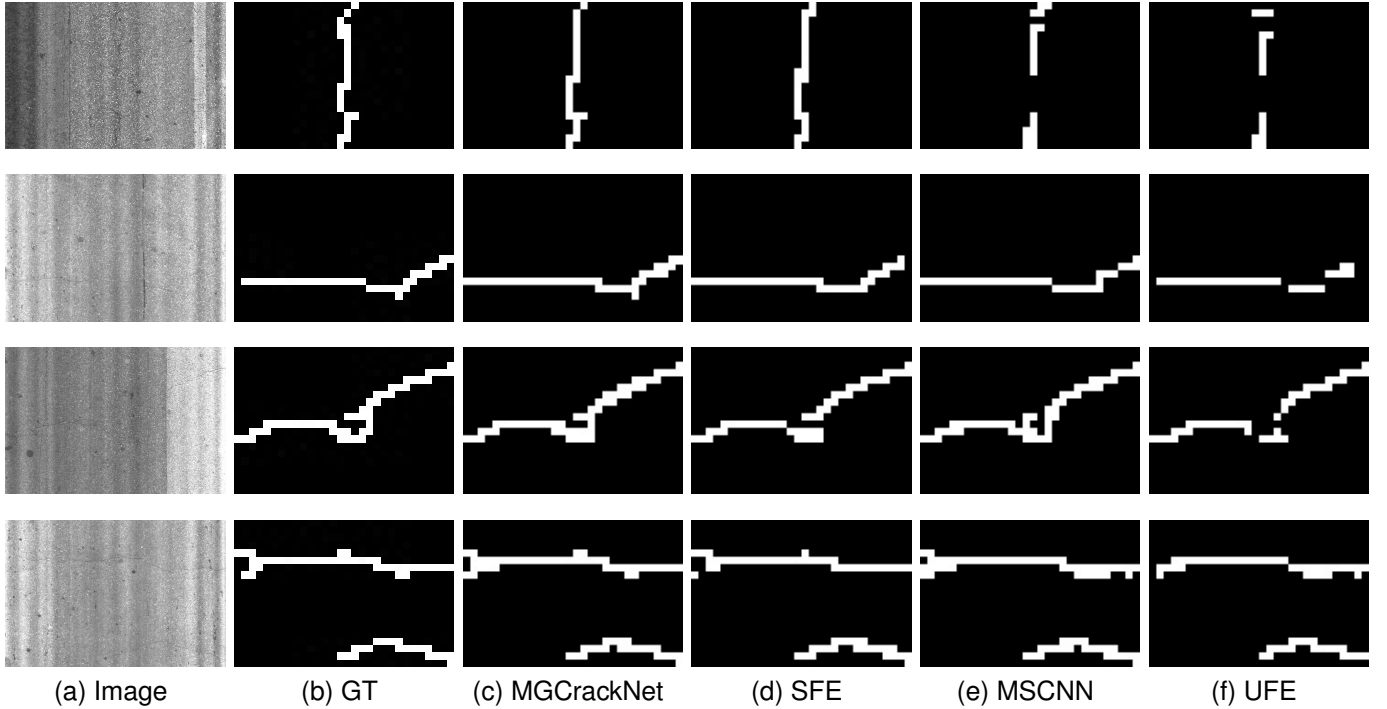


Fig. 6. Visual comparisons of the STOA methods and our methods on BPC. Please zoom out for more detailed cracks.

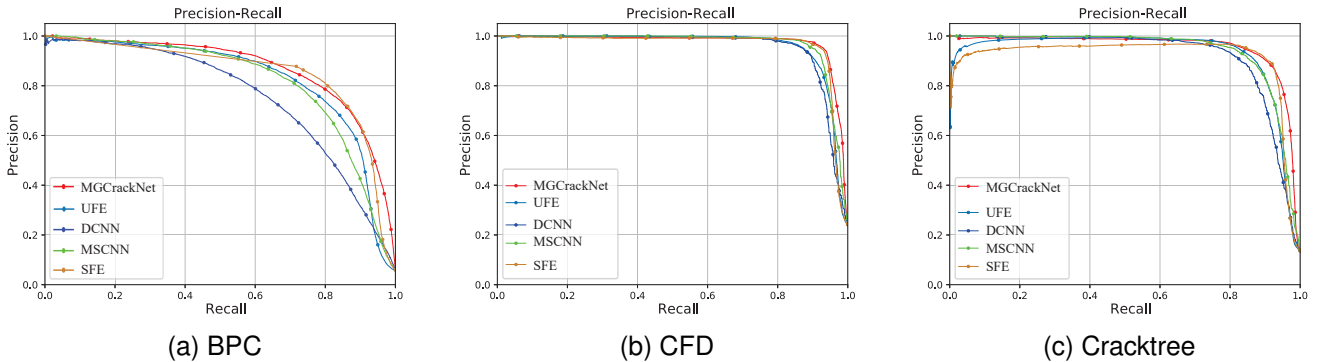


Fig. 7. The Precision-Recall curves of the crack detection methods on three datasets.

Tab. II shows our method consistently achieves the best performance with an 95.24% AP . In addition, the transformer also achieve over 80% AP on Cracktree dataset, indicating that it can handle crack datasets with less noise. However, the transformer is unable to fully fit the data features due to insufficient datasets, resulting in a significant decrease in classification results compared to CNN. As illustrated in Fig. 7 (c), our method consistently outperforms both local features based methods and global feature based ones. It means the proposed context flow have advantage to fuse both local and global features.

3) *Results on BPC*:: Tab. II shows the comparison results in terms of $F1$ and AP on BPC. There are two observations in Tab. II as follows:

- Our method achieves the best performances, *e.g.*

88.32% AP , significantly outperforming the other methods. Specially, the AP of DCNN, MSCNN, SFE and UFE are 12.48%, 8.12%, 3.22%, and 5.95% respectively, which are lower than that of our method. Besides, as illustrated in Fig. 7 that, MGCrackNet holds a curve most close to the up-right corner, achieving the best precision and recall values.

- The recall of our method (*i.e.*, 72.45%) is a lower than that of UFE (*i.e.*, 80.17%), while the precision of our method (*i.e.*, 86.90%) is a higher than that of UFE (*i.e.*, 76.23%). One possible reason is that MGCrackNet could capture more useful context information than UFE. Besides, BPC has a lot of noisy and blurry cracks, and even some crack patches are difficult for humans to be accurately labeled. Therefore, our method has a lower

TABLE III
ABLATION EXPERIMENTS ON BPC DATASET

SPDC	CG	MIL	P(%)	R(%)	F1(%)	AP(%)
✓	-	-	76.23	80.17	78.15	82.37
✓	✓	-	85.22	71.03	77.31	86.62
✓	✓	✓	86.90	72.45	79.02	88.32

TABLE IV
THE PERFORMANCE OF DIFFERENT DILATED RATES ON BPC DATASET

Dilated Rates	P(%)	R(%)	F1(%)	AP(%)
{1,2,3}	86.27	71.22	78.02	86.75
{1,2,5}	86.90	72.45	79.02	88.32
{1,3,5}	85.06	72.22	78.11	86.96
{2,3,5}	80.46	76.86	78.61	86.37

recall but higher precision to guarantee a higher AP than that of SFE, UFE, DCNN and MSCNN. Another possible reason is that although low-level features bring more detailed information, they also bring noisy information, especially for the stage S_3 .

F. Ablation Experiments

TABLE V
THE PERFORMANCE OF DIFFERENT POOLING OPERATION OF MIL MODULE ON BPC DATASET

Pooling	P(%)	R(%)	F1(%)	AP(%)
Max	86.27	72.06	78.53	87.67
Avg	86.90	72.45	79.02	88.32

An interesting observation in Tab. II is that the AP of three local feature-based networks (*i.e.*, DenseNet121 [32], ResNet50 [33] and VGG16 [34]) decline the performances with the increase of network depth. It indicates that crack does not require a larger receptive field to extract local context of cracks. Besides, the experimental results of transformer further validate the above explanation. The similarity between cracks and backgrounds make transformer [30] [31] inefficient for the BPC dataset. It indicates that increasing the discriminative ability of local features is more important.

Ablation Experiments for Each Module: As shown in Tab. III, the combination of each module improves the experimental results. Specifically, we first conduct experiments on the feature extraction stage of the PDC. We add the CG module to the PDC network, and the experimental results show that the gain of AP increased by 4.25%, demonstrating the effectiveness of that the semantic context should guide the local context. In addition, the MIL module gains a 1.7% increment in terms of AP , because it further optimizes the noise interference of the output results.

Robustness of Hyper-Parameters: To select the most appropriate hyper-parameters, we conduct a series of hyper-parameters experiments on the BPC dataset. The experimental

results are shown in Tab. IV. The results show that the hyper-parameter $r = 1, 2, 5$ has obtained the best experimental results.

Ablation Experiments for MIL Module: To further validate the impact of the different pooling operations on MIL, we experimentally select the two most commonly used pooling methods: max-pooling(Max) and avg-pooling (Avg), as shown in Tab. V. The avg-pooling achieves higher experimental results than that of max-pooling, gaining 0.65%. The reason is that the max-pooling only outputs the value with the highest probability, which captures the information of one sub-patch. On the contrary, the avg-pooling outputs the averaged prediction, which back-propagates gradients for all sub-patches. The continuous structure of cracks is a crucial factor to determine whether the patch contains cracks or not. Therefore, avg-pooling is more suitable for crack detection.

Visualization: We visualize some predicted results by our model and other approaches in Fig. 6. The images from BPC dataset contain some noises and a complex crack structure. Crack map outputted by MGCrackNet is very close to the ground truth, showing an excellent performance. As a contrary, other methods (*i.e.*, SFE, UFE, and MSCNN) have discontinuous predicted results. For instance, some non-cracked blocks are incorrectly predicted. Because the connection is very important to calibrate the damage degree of roads during the post-processing stage.

V. CONCLUSION

In this paper, we propose a MGCrackNet to handle the complex, irregular and non-discriminative cracks for bitumen pavement roads. From the perspective of leveraging context cues, multi-granularity contextual information is progressively fused by the multi-stage CG process for crack detection. In addition, we apply the MIL strategy to handle label misalignment problem. Experimental results on three crack datasets show that the proposed MGCrackNet achieves an excellent performance, demonstrating the effectiveness of our method.

Modeling context information is still an essential approach to handle crack problems. Meanwhile, we should introduce some methods to deal with both the noisy patches and labels. In the future, how to handle noises, and how to utilize unlabeled data are interesting directions.

REFERENCES

- [1] J. Fang, C. Yang, Y. Shi, N. Wang, and Y. Zhao, "External attention based transunet and label expansion strategy for crack detection," *IEEE Transactions on Intelligent Transportation Systems*, vol. 23, no. 10, pp. 19 054–19 063, 2022.
- [2] O. Ronneberger, P. Fischer, and T. Brox, "U-net: Convolutional networks for biomedical image segmentation," in *Medical Image Computing and Computer-Assisted Intervention—MICCAI 2015: 18th International Conference, Munich, Germany, October 5–9, 2015, Proceedings, Part III 18*. Springer, 2015, pp. 234–241.
- [3] X. Xiang, Z. Wang, and Y. Qiao, "An improved yolov5 crack detection method combined with transformer," *IEEE Sensors Journal*, vol. 22, no. 14, pp. 14 328–14 335, 2022.
- [4] H. Tsuchiya, S. Fukui, Y. Iwahori, Y. Hayashi, W. Acharyaviriya, and B. Kijirikul, "A method of data augmentation for classifying road damage considering influence on classification accuracy," *Procedia Computer Science*, vol. 159, pp. 1449–1458, 2019.
- [5] D.-P. Fan, G.-P. Ji, G. Sun, M.-M. Cheng, J. Shen, and L. Shao, "Camouflaged object detection," in *Proceedings of the IEEE/CVF conference on computer vision and pattern recognition*, 2020, pp. 2777–2787.

- [6] Z. Li, K. Xu, J. Xie, Q. Bi, and K. Qin, "Deep multiple instance convolutional neural networks for learning robust scene representations," *IEEE Transactions on Geoscience and Remote Sensing*, vol. 58, no. 5, pp. 3685–3702, 2020.
- [7] X. Wang, Y. Yan, P. Tang, X. Bai, and W. Liu, "Revisiting multiple instance neural networks," *Pattern Recognition*, vol. 74, pp. 15–24, 2018.
- [8] M. Ilse, J. M. Tomczak, and M. Welling, "Deep multiple instance learning for digital histopathology," in *Handbook of Medical Image Computing and Computer Assisted Intervention*. Elsevier, 2020, pp. 521–546.
- [9] F. Liu, J. Liu, and L. Wang, "Asphalt pavement crack detection based on convolutional neural network and infrared thermography," *IEEE Transactions on Intelligent Transportation Systems*, vol. 23, no. 11, pp. 22 145–22 155, 2022.
- [10] C. Han, T. Ma, J. Huyen, X. Huang, and Y. Zhang, "Crackw-net: A novel pavement crack image segmentation convolutional neural network," *IEEE Transactions on Intelligent Transportation Systems*, vol. 23, no. 11, pp. 22 135–22 144, 2021.
- [11] W. Choi and Y.-J. Cha, "Sddnet: Real-time crack segmentation," *IEEE Transactions on Industrial Electronics*, vol. 67, no. 9, pp. 8016–8025, 2019.
- [12] Z. Qu, C. Cao, L. Liu, and D.-Y. Zhou, "A deeply supervised convolutional neural network for pavement crack detection with multiscale feature fusion," *IEEE transactions on neural networks and learning systems*, vol. 33, no. 9, pp. 4890–4899, 2021.
- [13] C. Xiang, W. Wang, L. Deng, P. Shi, and X. Kong, "Crack detection algorithm for concrete structures based on super-resolution reconstruction and segmentation network," *Automation in Construction*, vol. 140, p. 104346, 2022.
- [14] W. Song, G. Jia, H. Zhu, D. Jia, L. Gao *et al.*, "Automated pavement crack damage detection using deep multiscale convolutional features," *Journal of Advanced Transportation*, vol. 2020, 2020.
- [15] Y. Liu, J. Yao, X. Lu, R. Xie, and L. Li, "Deepcrack: A deep hierarchical feature learning architecture for crack segmentation," *Neurocomputing*, vol. 338, pp. 139–153, 2019.
- [16] Z. Liu, X. Gu, H. Yang, L. Wang, Y. Chen, and D. Wang, "Novel yolov3 model with structure and hyperparameter optimization for detection of pavement concealed cracks in gpr images," *IEEE Transactions on Intelligent Transportation Systems*, vol. 23, no. 11, pp. 22 258–22 268, 2022.
- [17] H. Yao, Y. Liu, X. Li, Z. You, Y. Feng, and W. Lu, "A detection method for pavement cracks combining object detection and attention mechanism," *IEEE Transactions on Intelligent Transportation Systems*, vol. 23, no. 11, pp. 22 179–22 189, 2022.
- [18] K. Haciefendioğlu and H. B. Başağa, "Concrete road crack detection using deep learning-based faster r-cnn method," *Iranian Journal of Science and Technology, Transactions of Civil Engineering*, pp. 1–13, 2022.
- [19] T. S. Tran, V. P. Tran, H. J. Lee, J. M. Flores, and V. P. Le, "A two-step sequential automated crack detection and severity classification process for asphalt pavements," *International Journal of Pavement Engineering*, vol. 23, no. 6, pp. 2019–2033, 2022.
- [20] R. Li, J. Yu, F. Li, R. Yang, Y. Wang, and Z. Peng, "Automatic bridge crack detection using unmanned aerial vehicle and faster r-cnn," *Construction and Building Materials*, vol. 362, p. 129659, 2023.
- [21] N. Yusof, M. Osman, M. Noor, A. Ibrahim, N. Tahir, and N. Yusof, "Crack detection and classification in asphalt pavement images using deep convolution neural network," in *2018 8th IEEE international conference on control system, computing and engineering (ICCSCE)*. IEEE, 2018, pp. 227–232.
- [22] H. Feng, G.-s. Xu, and Y. Guo, "Multi-scale classification network for road crack detection," *IET Intelligent Transport Systems*, vol. 13, no. 2, pp. 398–405, 2019.
- [23] H. Wang, L. Qiu, J. Hu, and J. Zhang, "I2cnet: An intra- and inter-class context information fusion network for blastocyst segmentation," pp. 1415–1422, 2022.
- [24] L. Duan, J. Zeng, J. Pang, and J. Wang, "Pavement crack detection using multi-stage structural feature extraction model," in *2021 IEEE International Conference on Image Processing (ICIP)*. IEEE, 2021, pp. 969–973.
- [25] P. Wang, P. Chen, Y. Yuan, D. Liu, Z. Huang, X. Hou, and G. W. Cottrell, "Understanding convolution for semantic segmentation," *CoRR*, vol. abs/1702.08502, 2017. [Online]. Available: <http://arxiv.org/abs/1702.08502>
- [26] D.-P. Fan, G.-P. Ji, M.-M. Cheng, and L. Shao, "Concealed object detection," *IEEE Transactions on Pattern Analysis and Machine Intelligence*, vol. 44, no. 10, pp. 6024–6042, 2021.
- [27] H. Mei, G.-P. Ji, Z. Wei, X. Yang, X. Wei, and D.-P. Fan, "Camouflaged object segmentation with distraction mining," in *Proceedings of the IEEE/CVF Conference on Computer Vision and Pattern Recognition*, 2021, pp. 8772–8781.
- [28] Y. Shi, L. Cui, Z. Qi, F. Meng, and Z. Chen, "Automatic road crack detection using random structured forests," *IEEE Transactions on Intelligent Transportation Systems*, vol. 17, no. 12, pp. 3434–3445, 2016.
- [29] Q. Zou, Y. Cao, Q. Li, Q. Mao, and S. Wang, "Cracktree: Automatic crack detection from pavement images," *Pattern Recognition Letters*, vol. 33, no. 3, pp. 227–238, 2012.
- [30] Z. Liu, Y. Lin, Y. Cao, H. Hu, Y. Wei, Z. Zhang, S. Lin, and B. Guo, "Swin transformer: Hierarchical vision transformer using shifted windows," in *Proceedings of the IEEE/CVF international conference on computer vision*, 2021, pp. 10 012–10 022.
- [31] J. Yang, C. Li, P. Zhang, X. Dai, B. Xiao, L. Yuan, and J. Gao, "Focal self-attention for local-global interactions in vision transformers," *arXiv preprint arXiv:2107.00641*, 2021.
- [32] G. Huang, Z. Liu, L. Van Der Maaten, and K. Q. Weinberger, "Densely connected convolutional networks," in *Proceedings of the IEEE conference on computer vision and pattern recognition*, 2017, pp. 4700–4708.
- [33] K. He, X. Zhang, S. Ren, and J. Sun, "Deep residual learning for image recognition," in *Proceedings of the IEEE conference on computer vision and pattern recognition*, 2016, pp. 770–778.
- [34] K. Simonyan and A. Zisserman, "Very deep convolutional networks for large-scale image recognition," *arXiv preprint arXiv:1409.1556*, 2014.
- [35] J. Pang, B. Xiong, P. Li, and J. Wu, "You need dilated convolution for pavement crack detection," in *2022 China Automation Congress (CAC)*. IEEE, 2022, pp. 899–904.
- [36] A. Dosovitskiy, L. Beyer, A. Kolesnikov, D. Weissenborn, X. Zhai, T. Unterthiner, M. Dehghani, M. Minderer, G. Heigold, S. Gelly, J. Uszkoreit, and N. Houlsby, "An image is worth 16x16 words: Transformers for image recognition at scale," 2021.